# Chapter 4
# Multi-Functional Systems Based on Shear Thickening Fluid

**Xinglong Gong, Junshuo Zhang, and Shouhu Xuan**

## 4.1 Introduction

Shear thickening fluids (STFs) are dense granular suspensions with a drastic increase in viscosity as shear rate or stress increases and exceeds the critical shear rate [1–4]. When the applied loading is released, the viscosity would return to its initial state reversibly. In recent years, a large number of studies have been carried out on studying the rheological properties of STF, and several shear thickening mechanisms, e.g., ordered-disorder transition [5, 6], hydrocluster mechanism [7–10], and contact force [11–13], have been proposed. Although there is no unified explanation about the shear thickening mechanism, the STFs have been widely used in engineering due to their unique mechanical properties.

As an excellent energy-absorbing material, the traditional STFs have been applied in various damping systems. Typically, it was expected to enhance the anti-impact properties of textile-based armor. Wagner's et al. [14] firstly developed STF-based body armor by impregnating STF with high performance fabrics. It was found that the bulletproof performance of Kevlar fabric could be significantly improved by introducing STFs [15–25]. STF also can be integrated into damping systems to optimize and improve the dynamic performance [26–31]. Moreover, STF has been used in medical equipment to provide protection against external physical shocks [32].

Besides the traditional shear rate–dependent mechanical behavior, some types of STFs have special properties, such as shear thickening effects increased with temperature [33, 34] or color changed in response to external forces [35], which demonstrate an application potential in multi-functional devices. By adding conductive

X. Gong · J. Zhang · S. Xuan (✉)
Department of Modern Mechanics, University of Science and Technology of China, Hefei, China
e-mail: xuansh@ustc.edu.cn



S. Gürgen (ed.), *Shear Thickening Fluid*,
https://doi.org/10.1007/978-3-031-25717-9_4

materials, such as carbon nanotubes, carbon black, and graphene, or using ionic liquids [36] as dispersants [37–41], the STF not only exhibits an enhanced shear thickening performance but also possesses typical electrical conductivity. Therefore, the conductive STFs show sensing function and can be further applied in wearable devices. As a result, the multi-functional STFs exhibit wide potential in smart devices and structures by improving the mechanical and electrical properties of smart structures [42, 43]. In this chapter, a detailed overview of STF applications is given after a brief introduction to the multi-functional STF.

## 4.2 Multi-Functional STF

The shear thickening performance of STF is directly associated with the function and properties of dispersed phase and dispersed medium. Moreover, the additives also affect the rheological behavior of STF. Therefore, by adjusting the dispersed particles and carrier liquid, or using additives, STF can be endowed with multi-field coupling performance, such as force-thermal, force-optical, and force-electric coupling properties.

### *4.2.1 Traditional STF*

The traditional STFs are prepared by dispersing uniform particles into disperse phase. The properties of STF are highly dependent on the dispersed phase, the dispersed media, and the additives. The rheology of STF is dramatically affected by the dispersed phase, such as volume fraction, particle size, size distribution, shape, and surface chemistry properties [44–47].

The dispersed phases used in shear thickening studies generally fall into two categories. The first category is inorganic particles, including clay, limestone, quartz powder, iron oxide pigment, silica, etc. [48–52]. The second category is organic particles, including cornstarch particles, polyvinyl chloride (PVC), polystyrene ethyl acrylonitrile (PS-AN), polystyrene (PSt), polymethyl methacrylate (PMMA), polystyrene ethyl acrylate (PST-EA), etc. [53–57].

Besides these factors itself, additive particles also exhibit a great influence on shear thickening mechanism. Various research teams carried out intensive works on shear thickening behavior by adding additive particles to the suspension [58–62]. Yang et al. [45] studied the pH-dependent rheological properties of titanium dioxide mixtures by adding $HNO_3$ or NaOH to change the particle surface charge. Gürgen et al. [58] added ceramic particles to silicon-based STF and found that ceramic particles in STF would reduce the shear thickening performance of STF, and the degree of reduction depended on the amount of additives and particle size, etc.

Ye et al. [62] studied the effect of surfactants on shear thickening behavior of STF by adding cationic, anionic, nonionic, and zwitterionic surfactants into STF. The results show that the surfactant affects the shear thickening rheology by altering the inter-particle and surface forces.

### *4.2.2 STF with Force-Thermal Coupling Characteristics*

Shear thickening phenomenon is depended on fluid lubrication, frictional contact between particles, hydrogen bonding between particles and dispersed media. Generally, the shear thickening effect of STF decreases with increasing temperature [63–66]. However, by modifying the surface of dispersed particles or adding additives, the force between particles changes so that the shear thickening effect can be enhanced with the increase of temperature. Hsu et al. [33] prepared a silica colloid with different surface roughness at different temperatures. As shown in Fig. 4.1, the

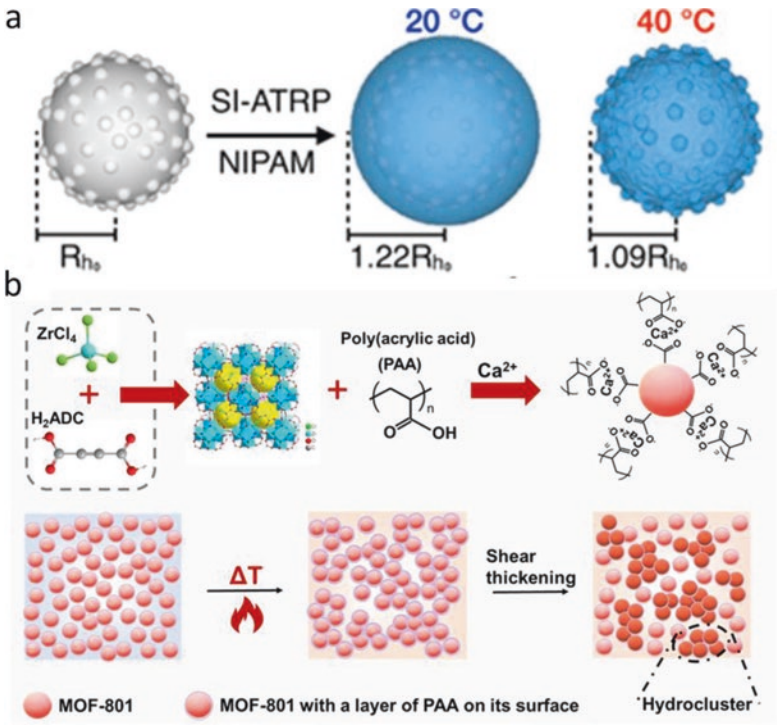


**Fig. 4.1** (**a**) Schematics of the PNIPAM-grafted rough (RB) particles at 20 °C and 40 °C [33]. (**b**) Schematic diagram of M-STF shear thickening effect enhancement [34]. Reprinted by permission from Elsevier

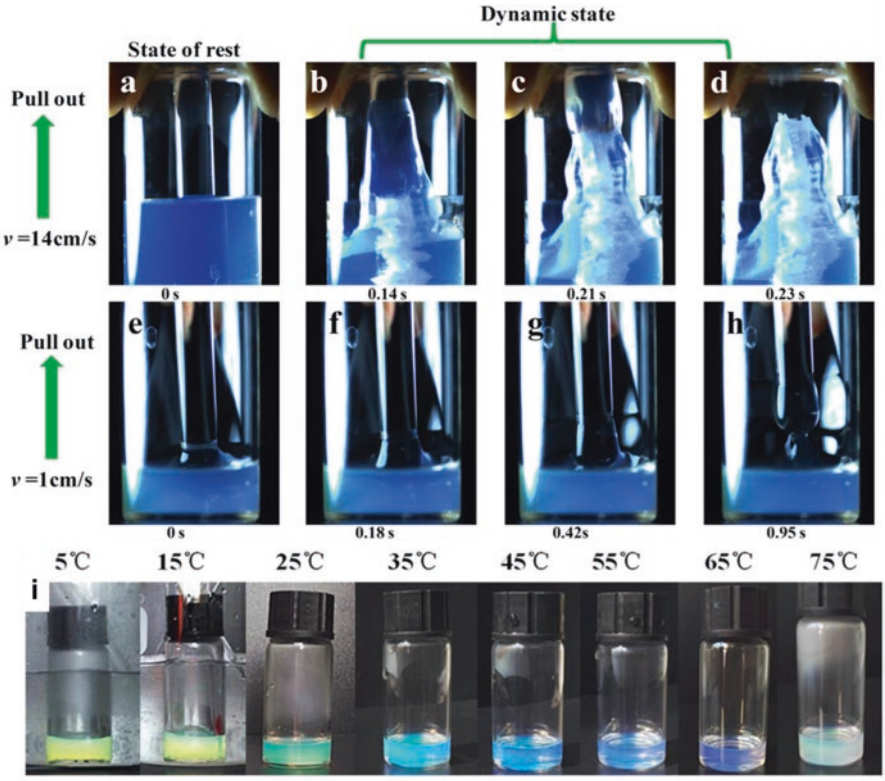


**Fig. 4.2** The photographs taken when the glass bar was pulled out from the c-STF using fast speed (**a**–**d**) and low speed (**e**–**h**). (**i**) Photographs of the color changes in c-STF (the average diameter of $SiO_2$ nanospheres was about 200 nm) with the temperature changing [35]. Reprinted by permission from IOP Publishing

surface roughness of PNIPAM particles at 40 °C is greater than that at 20 °C. As a result, the shear thickening effect of STF prepared by PNIPAM particles at 40 °C is higher than that at 20 °C. Recently, Wu et al. [34] reported a new MOF-801-based STF with better thickening effect at high temperature based on the thermal resistance mechanism of thermophilic proteins (Fig. 4.2). MOF-801, which is rich in carboxyl groups on the surface, was used as the dispersed phase and added into the polyethylene glycol (PEG). By introducing polyacrylic acid (PAA) and $Ca^{2+}$ into the dispersed medium, the hydrogen bonding, which is the internal force for the conventional STF, was replaced with the ionic and hydrophobic interactions. As a result, a novel MOF-801-based STF (M-STF) with enhanced shear thickening properties was developed at elevated temperature for the first time.

### 4.2.3 STF with Force-Optical Coupling Characteristics

Photonic crystals have become one of the most representative color materials because of their long-range ordered periodic microstructures. However, the color variation depends largely on the angle of view. [67, 68]. $SiO_2$ nanospheres can be synthesized by the Stöber hydrolysis technique [69–71], which is the most commonly used material for preparing STF, and it is also a photonic crystal material. However, in most cases, the polydispersity index (PDI) of $SiO_2$ nanospheres is not sufficiently small, and the surface chemical properties and refractive indexes of the $SiO_2$ are different from carrier fluid, which results in the opacity of STF.

Liu et al. [35] obtained $SiO_2$ nanospheres with PDI within 5% by controlling experimental conditions. Importantly, the $SiO_2$ was only cleaned with ethanol and the surface contained rich ethanol hydroxyl, which had good compatibility with PEG 200. In addition, the $SiO_2$ and PEG200 should have the same refractive index. As a result, the semitransparent and colorful STFs were obtained and the color of STF was related to the size and amount of $SiO_2$ particles. STF with different colors (c-STF) could be obtained by controlling the size and volume fraction of $SiO_2$ particles. Interestingly, the c-STF also changed its color under external loads. When the glass rod was pulled quickly (Fig. 4.2b-c) from the c-STF, the color changed from the initial translucent blue (Fig. 4.2a) to white. However, when the external influence was mild, there was no significant state and color change. The c-STF also showed different colors at different temperatures (Fig. 4.2i). Clearly, the ability to change color under different conditions endowed the STF with wide potential application in multi-functional soft armor defense materials.

### 4.2.4 STF with Force-Electric Coupling Characteristics

The CNTs exhibit great electrical conductivity, mechanical properties, and low density characteristics, and thus they are ideal nano-additives to reinforce and functionalize conventional materials [72–76]. By introducing CNTs into the dispersion, the conductive STF is obtained. In addition, as the networks formed by CNT restrict the particle motions, the thickening effect is enhanced [39–41]. The homogeneously dispersed CNTs within the $SiO_2$-based STF can be assembled to create conductive paths, thereby presenting typical electrical conductivity [77–79]. Therefore, it shows high potential in the field of wearable devices.

Moreover, the ionic liquid has a good chemical stability, thermal stability, low volatility, and electrical conductivity. It is suitable as a dispersed medium to fabricate high-performance STF with unique mechanic-conductive coupling performance. Qin et al. [36] used four ionic liquids, 1-Butyl-3-Methylimidazolium Tetraf luoroborate, 1-Butylpyridinium Tetrafluoroborate, 1-Butyl-3-Methylimidazolium Hexafluorophosphate, 1-Ethoxyl-3-Methylimidazolium Tetrafluoroborate, as the

dispersion medium to prepare a new type of shear thickening fluid. The electrical conductivity of STF was suppressed by including more silica microsphere in the suspension. When the concentration of silicon microsphere was 64%, the electrical conductivity of STF was about 2500 μS/cm (Fig. 4.5j). This kind of shear thickening fluid has a clearer shear thickening effect and has an excellent electric conductivity and thermal stability. It can be further interpreted into the Kevlar fabric and thus the smart body armor is developed.

## 4.3 Applications of the Multi-Functional STF Systems

In addition to the development of multi-functional STFs, STFs are also used as reinforcement materials for multi-functional systems. For example, the STFs can be used in lithium batteries, supercapacitors, motion sensors, and triboelectric nanogenerator (TENG) devices to improve the mechanical and electrical properties of smart structures.

### *4.3.1 Shear Thickened Electrolyte*

Lithium ion batteries have been developed for several engineering applications ranging from biomedical devices to new energy vehicles [81–88]. Currently, commercial lithium ion batteries mostly use flammable electrolytes such as ethylene carbonate, propylene carbonate, and dimethyl carbonate [89–91]. However, when the electrolytes receive an impact damage, they may show spontaneous thermal reactions, fires, and explosions. Therefore, it is very important to enhance the impact resistance of electrolyte.

By adding fumed silica nanoparticles to a commercial electrolyte (1 M $LiFP_6$ in EC/DMC), Ding et al. [92] developed a multi-functional fluid with thickening properties that provide impact protection inherent to lithium ion batteries while serving as a highly conductive electrolyte in lithium-ion batteries. Typically, the conductivity of the STF electrolytes was higher compared to commercial electrolytes. As shown in Fig. 4.3a, the maximum conductivity increase for 1 M $LiPF_6$ in EC/DMC (1:1) is observed for the STF having a silica loading of 10.7 wt.%, with the value of $1.93 \times 10^{-2}\ \Omega^{-1}\ cm^{-1}$, which was greatly higher than the commercial electrolyte with no addition of fumed silica ($2 \times 10^{-3}\ \Omega^{-1}\ cm^{-1}$).

Furthermore, lithium-ion batteries using STF electrolytes provide enhanced capacity at high charge and discharge rates, and the batteries using STF electrolytes maintain their electrochemical capacity after successive impact conditions. As shown in Fig. 4.3b, lithium-ion batteries using STF electrolytes can withstand a shock energy up to 0.568 J, which is higher than 0.426 J that can be safely tolerated by lithium-ion batteries with normal electrolyte. Figure 4.3c-e shows the protective mechanism of STF electrolyte under impact conditions. It is seen that the silica

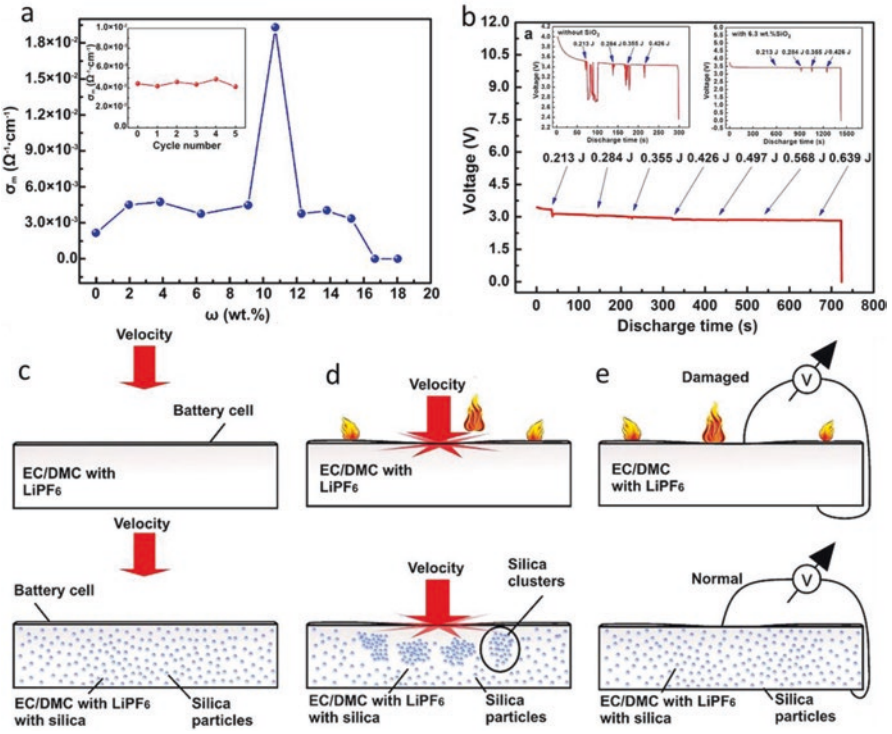


**Fig. 4.3** (**a**) Room temperature variation of ionic conductivity of composite electrolytes ($SiO_2$/$LiPF_6$ in EC/DMC) versus weight fraction (ω) of fumed silica. Inset: Ionic conductivity of composite electrolyte with 9.1 wt.% $SiO_2$ after impact tests. (**b**) Discharge curve of $LiFePO_4$ electrode in the STF electrolyte of EC/DMC/$LiPF_6$ with 9.1 wt.% $SiO_2$. Impacts with different energies were applied to the cell during the discharge. For comparison, the discharge curves of $LiFePO_4$ electrode in bare EC/DMC/$LiPF_6$ electrolyte and composite electrolyte of EC/DMC/$LiPF_6$ with 6.3 wt.% $SiO_2$ (showing shear thinning effect) are also shown in the inset of (**b**). (**c**–**e**) Schematic representation of the protective mechanism of STF electrolyte [92]. Under the Creative Commons license

particles enhance the ionic conductivity due to their mutual repulsion. When the electrolyte is impacted, the silica nanoparticles overcome the inter-particle repulsive force and aggregate in the electrolyte, causing the electrolyte to be solid and show typical shear thickening phenomenon, resulting in the increase of suspension viscosity. Hooke's model proposes that the increase in viscosity slows down the energy dissipation due to the basic function of restoring force. The overall effect of this phenomenon is to slow down the rise in electrolyte temperature after impact and effectively increase the stiffness of the battery. Conversely, battery systems without shear thickening function are prone to undergo large deformations and a quick jump in temperature during the impact, igniting the solvent.

Liu et al. [93] developed an electrochemically stable shear thickening electrolyte to enhance the protection of LIBs. The electrolyte was designed by the integration of (3-aminopropyl)triethoxysilane (APTES) modified glass fiber additives and

typical liquid electrolyte. Compared with conventional electrolytes, shear thickening electrolytes behaved as solid materials on impact, preventing bullets from penetrating them. The half cells with STF electrolytes showed great cyclability, in which the capacity retention rate of STF electrolytes half battery was 95.2% after 500 cycles, while the capacity retention rate of conventional electrolytes half battery was 61.1% after 500 cycles. This phenomenon was most likely due to the functionalized glass fibers (mGFs) in STF electrolyte, which may be attributed to form torturous structure and slow down lithium dendrite growth. In order to further evaluate the impact resistance of STF electrolytes in the battery, the LFP-LTO bag battery with STF electrolytes was prepared. A steel ball was impacted on the bagged battery and the open-circuit voltage (OCV) of the bagged battery was tracked in real time. The voltage of the cell with the STF electrolytes was more stable than that of the bag cell with the conventional electrolytes. The impact test of the battery showed that the impact resistant battery can be realized by using STF electrolytes.

Recently, Wu et al. [94] developed an STF-filled organic gel electrolytes (PVA/STF) to prepare STF-enhanced supercapacitor (SSC). Due to the shear thickening rheology, the enhancement of $SiO_2$, and the hydrogen bonding in the PVA matrix, PVA/STF dissipates a large amount of energy during the impact process.

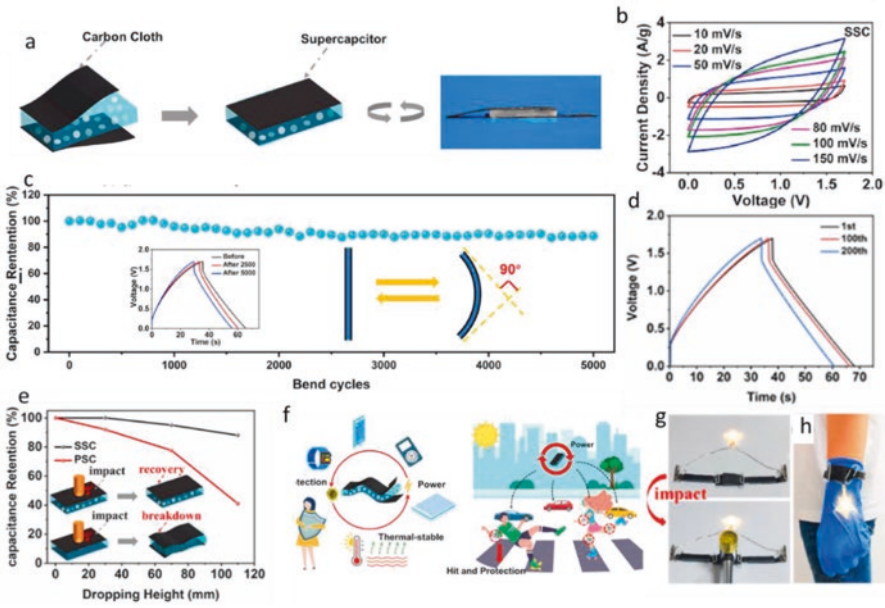


**Fig. 4.4** (**a**) Schematic diagram and photograph of SSC. (**b**) CV curves of SSC. (**c**) Capacitance stability of the SSC after a number of bending cycles. (**d**) Capacitance stability of the SSC after a number of compression cycles. (**e**) Capacitance retention of SSC and PSC after different collisions. Insets: schematic diagram of SSC and PSC under impact. (**f**) Practical applications of SSC in daily life. (**g**) Photographs of the circuit with three SSCs before and after impact. A wearable wristband composed of three SSCs is used as (**h**) an energy storage device [94]. Reprinted by permission from Elsevier

Figure 4.4a shows the manufacturing steps for SSC, which is obtained by sandwiching PVA/STF between two carbon cloth clips. The voltage window of the SSC is extended to 1.7 V (Fig. 4.4b), almost twice that of a traditional hydrogel-based supercapacitor. SSC also has good bending and compression cycle stability. After bending to 90° for 5000 times, only 11% specific capacitance attenuation is observed (Fig. 4.4c). After 200 compression cycles, it still retains 90% capacitance (Fig. 4.4d). In addition, SSC has a good environmental stability and thermal stability. Due to the excellent impact resistance of the PVA/STF, the SSC maintains its integrity after impact with minimal capacitance loss. When the hammer drop height is 110 mm, the capacitance loss of SSC is only 12%, while the loss of ordinary hydrogel capacitor is 59% (Fig. 4.4e), illustrating the good capacitance retention of SSC. According to the results, SSC can be employed as a power source while providing flexible body protection (Fig. 4.4f). In addition, the SSC can be bent into a wristband as a wearable energy storage device (Fig. 4.4g-h). It can also protect humans from shock excitation. Therefore, SSC with good energy storage performance, high flexibility, and excellent mechanical properties shows broad application prospects in wearable devices, new power supplies, and protective structures.

### *4.3.2 Wearable Devices with STF*

Nowadays, flexible sensors have attracted great attention due to their wide range of applications in wearable devices [95–97]. Flexible sensors can be applied to electronic skin, touch sensing, health motion detection, soft robots, etc. [98–104]. In addition, the STF has been applied in flexible sensors to improve the mechanical and electrical properties. In this case, Liu et al. [80] reported on a CNT-/STF-/Kevlar-based wearable electronic textile (ET) with sensing capabilities and protective properties. The yarn pull-out and stab resistance tests showed that the anti-impact performance of this material is improved due to the STF and CNT fillers. Compared to the neat textiles, the ET composite exhibited two times larger in peak impact force and 50% increment in the stab resistance. This indicates that the ET composite can be efficiently used under energy absorbing and anti-impact conditions. ET is conductive due to CNT addition into the composite material, and thus the prepared ET not only has an excellent protection performance but also shows excellent sensing characteristics. Figure 4.5a-b shows a conductive circuit consisting of ET fabric, LED bulb, and battery. When the circuit is connected, the LED bulb lights up, proving that the ET has a good electrical conductivity. Figure 4.5c-e shows the change in normalized resistance during the cyclic bending test. The results showed that the response signals under different bending angles and frequencies are distinguishable and stable after repeated cycles. Due to its high sensitivity to deformation, flexible ET can be used to monitor human movement. As shown in Fig. 4.5f-g, ET can clearly identify the movements of fingers and elbow joints, indicating that ET sensors have the potential to be applied to detect various movements of human or robot bodies. Figure 4.5h-i shows the sensing mechanism of ET. When

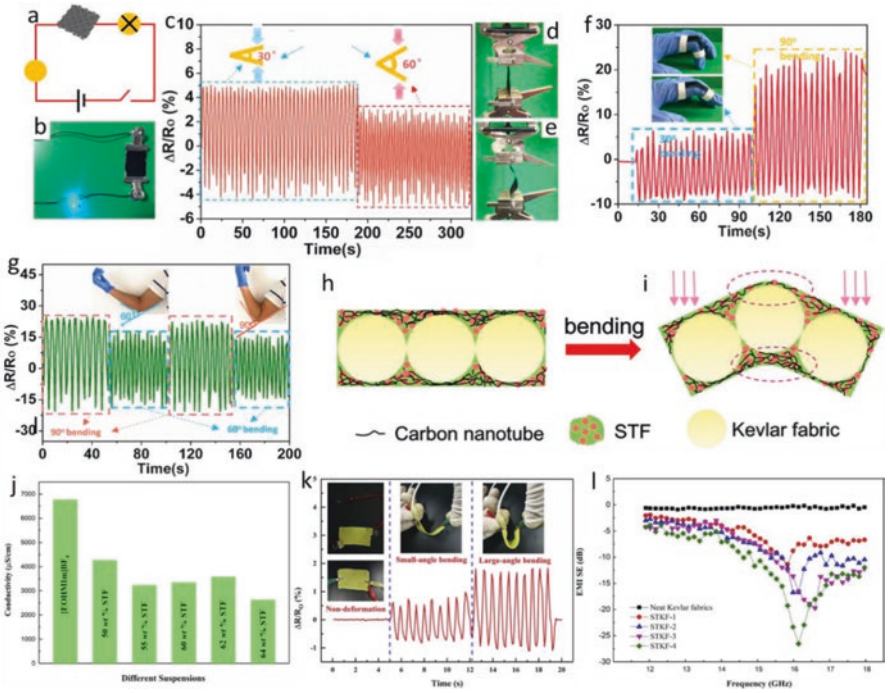


**Fig. 4.5** Illustration (**a**) and photograph (**b**) of a conductive circuit composed of the ET fabric, an LED bulb, and a cell. Normalized resistance changes ($\Delta R/R_0$) of the ET sensor during a cyclic bending test (**c**). Photographs of the ET sensor on a steel clamp that undergoes a bending test (**d** and **e**). Relative normalized resistance change of the ET in monitoring movements of finger (**f**) and elbow at different angels (**g**). The illustration of partial magnification of the cross section of the yarns of the CNT/STF/Kevlar composite (**h** and **i**) [80]. (**j**) Conductivity for [EOHMIm] [$BF_4$] STFs with different concentrations of silica microsphere. (**k**) Normalized electrical resistance versus time for the STKF-3 during different bending circles and static non-deformation, respectively. (**l**) EMI SE dependencies of frequency for the STKF and the neat Kevlar fabric [36]. Reprinted by permission from Elsevier

CNT/STF/Kevlar composites are bent by external forces, some parts of CNT conductive paths are destroyed. In addition, when ET returns to its original shape, the conductive path also quickly recovers by the effect of fluidity. Therefore, the conductivity of ET sensor has a significant repeatability under external stimuli.

Qin et al. [36] developed a soft armor material (STKF) which is constructed by high-performance textiles treated with a recently developed STF composed of silica microsphere and ionic liquids (ILs). Besides the resistance to external loading, the STKF exhibits a stable electrical conductivity and high sensitivity to the applied deformation, which can be used to monitor the human body motions. The ILs are used as dispersion medium to prepare STF with a high electrical conductivity. As shown in Fig. 4.5k, the LED bulb is lighted up in a circuit composed of STKF, proving the conductivity of STKF. At the same time, the resistance of STKF is highly sensitive to the applied deformation, which provides an opportunity to develop new

types of armor with excellent protection and intelligent wearable characteristics. In addition, due to the good electrical conductivity of STKF, it has a certain EMI SE level, which can reach 27 dB near the 16 GHz frequency (Fig. 4.5l).

Zhang et al. [42] designed a novel STF/Ecoflex composite by encapsulating STF in Ecoflex-0030. The compression and drop tests proved that STF/Ecoflex composite has excellent impact resistance, and the increase in the STF amount is helpful to enhance the anti-impact behavior of the composite. The STF can be conductive by including CNTs into the suspension. Therefore, conductive STF/Ecoflex (C-STF/Ecoflex) with sensing properties under different conditions is designed by including CNTs into the STF. As shown in Fig. 4.6a, the electrical response of C-STF/Ecoflex becomes apparent as the compression displacement increases. In addition, C-STF/Ecoflex can respond to the impact signals in time under impact conditions (Fig. 4.6b), and its resistance that changes under impact conditions is directly related to the impact energy (Fig. 4.6c), indicating that C-STF/Ecoflex has the potential to be used as a sensor with protective capabilities under impact conditions. Then, the wearable multi-functional protective suit C-STF/Ecoflex/Kevlar is developed by

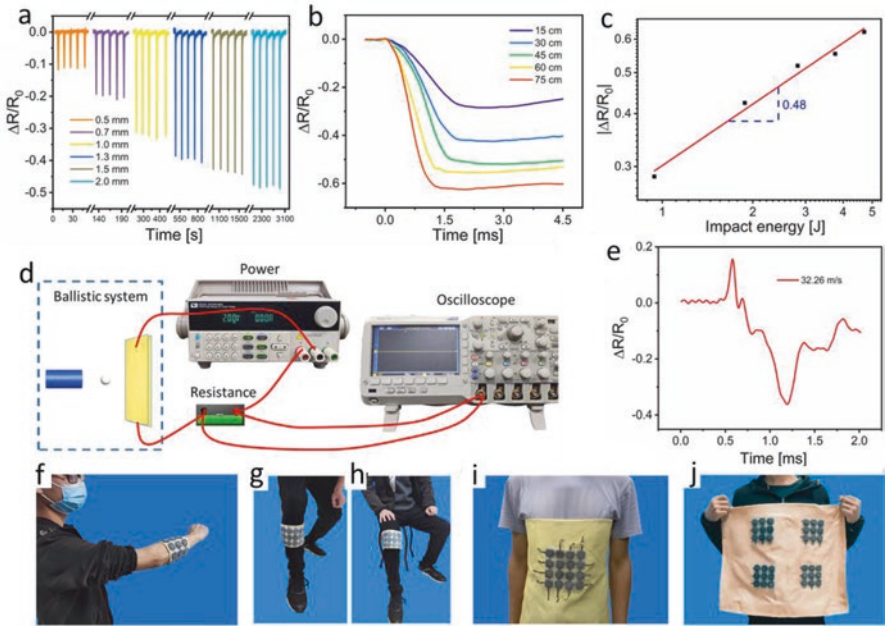


**Fig. 4.6** (**a**) Resistance change rate under different compression displacements. (**b**) The $\Delta R/R_0$vs. time curves when the hammerhead fell from different heights. (**c**) The fitting curve of $|\Delta R/R_0|$ with impact energy in the logarithmic coordinate system. (**d**) Schematic of the system for recording the variation of C-STF/Kevlar resistance during the high-speed impact. (**e**) The curves of the resistance signal of C-STF/Kevlar under 32.26 m/s. Shape programmable photographs of C-STF/Ecoflex/Kevlar device: (**f**) worn on arm, (**g**) worn on leg, (**h**) worn on knee, (**i**) the overlying one provided higher protection effect, and (**j**) the arrays were integrated into one pad with larger protection area [42]. Reprinted by permission from Elsevier

combining C-STF/Ecoflex and Kevlar. Ballistic impact tests show that C-STF/Ecoflex/Kevlar can sense the impact behavior of projectiles (Fig. 4.6d-e). In addition, C-STF/Ecoflex/Kevlar is flexible and lightweight, which can be comfortably worn on people's arms (Fig. 4.6f), legs (Fig. 4.6g), knees (Fig. 4.6h), and waist (Fig. 4.6i). By bringing the four arrays together (Fig. 4.6j), a large scale area can be obtained. Therefore, C-STF/Ecoflex/Kevlar can be used as an intelligent wearable device with protective characteristics.

### *4.3.3 TENG Based on STF*

More wearable electronic devices have been developed for daily life use. A battery is required to supply power to the wearable devices; however, the need of charge or replace of the power unit has been a challenging issue, apart from their heavy structures [105]. For this reason, triboelectric nanogenerators (TENGs) have been rising as a promising energy conversion device due to a list of advantages such as lightweight, easy fabrication, and low cost [106–113]. However, in order to obtain energy, TENG needs to maintain various mechanical excitation for a long time, such as compression, distortion, and friction, which is easy to damage the TENG equipment. Because of its unique shear thickening properties, the introduction of STF into TENG equipment is expected to enhance the structural durability and impact resistance of TENG equipment.

Wang et al. [43] developed a multi-mode energy-harvesting and safeguarding STF-based TENG (Fig. 4.7a-e). The TENG exhibits a high-energy harvesting effect in which the maximum power density is about 27.05 $mW/m^2$ under compression. As STF flows into the TENG, it rubs against the polymer, causing electron conversion and output current (Fig. 4.7f-h). Therefore, this portable TENG shows the potential of perceiving human movement due to the difference in amplitude and frequency of movement during human moving. In addition, the Ecoflex/CI housing can be magnetically driven to deform, collecting mechanical energy and outputting voltage signals during deforming (Fig. 4.7i). Because of the shear thickening property of STF, the TENG has a good protective performance. A drop hammer test is used to investigate the protective properties of TENG. Figure 4.7j shows that TENG has the lowest impact force. In addition, the TENG output voltage increases with the increase of impact height (Fig. 4.7k). These results indicate that TENG can be used as a protective self-supplied power sensor. Here, a TENG-based human hand array is developed (Fig. 4.7l). TENGs are able to detect bending excitation (Fig. 4.7m-n), and they can detect pressure in real time for finger bending, grasping ring boxes and apples. In addition, the wearable Kevlar/TENG composite fabric has been developed (Fig. 4.7o). The Kevlar/TENG composite with wearable shape adaptability has self-powered characteristics and protective effects, which can be used as intelligent clothing in the fields of robotics, human-computer interaction, healthcare, and protection. In conclusion, the STF-based TENG exhibits significant potentials in power sources, healthcare, smart systems, and safeguards.

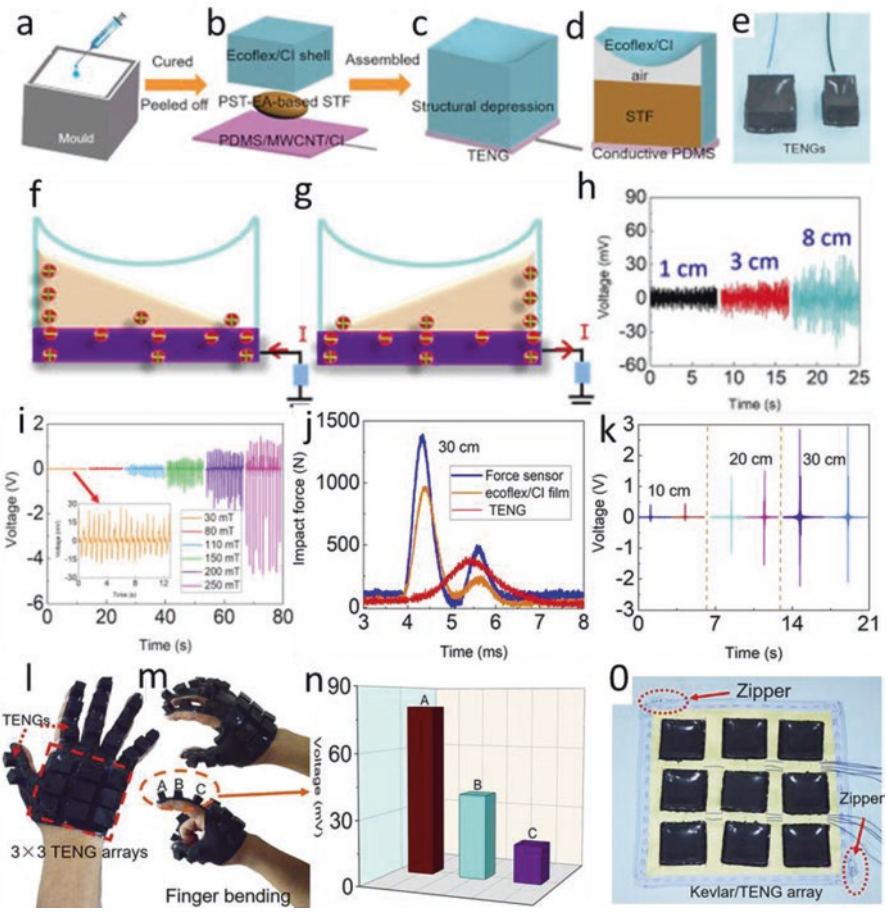


**Fig. 4.7** (**a**) Preparation procedures of the TENG device: uncured Ecoflex/CI were dropped on the mold, (**b**, **c**, **e**) STF, Ecoflex/CI, and PDMS/MWCNT/CI were assembled and cured into TENG, (**d**) schematic of the components of TENG. (**f**, **g**) Electrons transferred during STF flowing process and (**h**) the corresponding voltages. (**i**) Magnetic-dependent triboelectric performance. (**j**) Representative force curves comparison of TENG, Ecoflex/CI, and force sensor impacted from 30 cm height. (**k**) The corresponding triboelectric voltages of TENG during loading process. (**l**) A TENG-based hand array, human gesture sensing performance of the device: (**m**) index finger bending and (**n**) the corresponding maximum voltages. (**o**) The wearable Kevlar/TENG array [43]. Reprinted by permission from Elsevier

Yun et al. [114] developed an STF-TENG benefitting from the shear thickening rheology (Fig. 4.8a). The STF-based TENG shows an inherent anti-impact performance, which is tested by dropping a steel ball on the device dropped from different heights. Durability tests for contact separation are also carried out and the output voltage does not decrease up to 102,600 cycles, indicating structural reliability and long-term durability of the STF-based TENG. An STF-TENG is able to monitor the

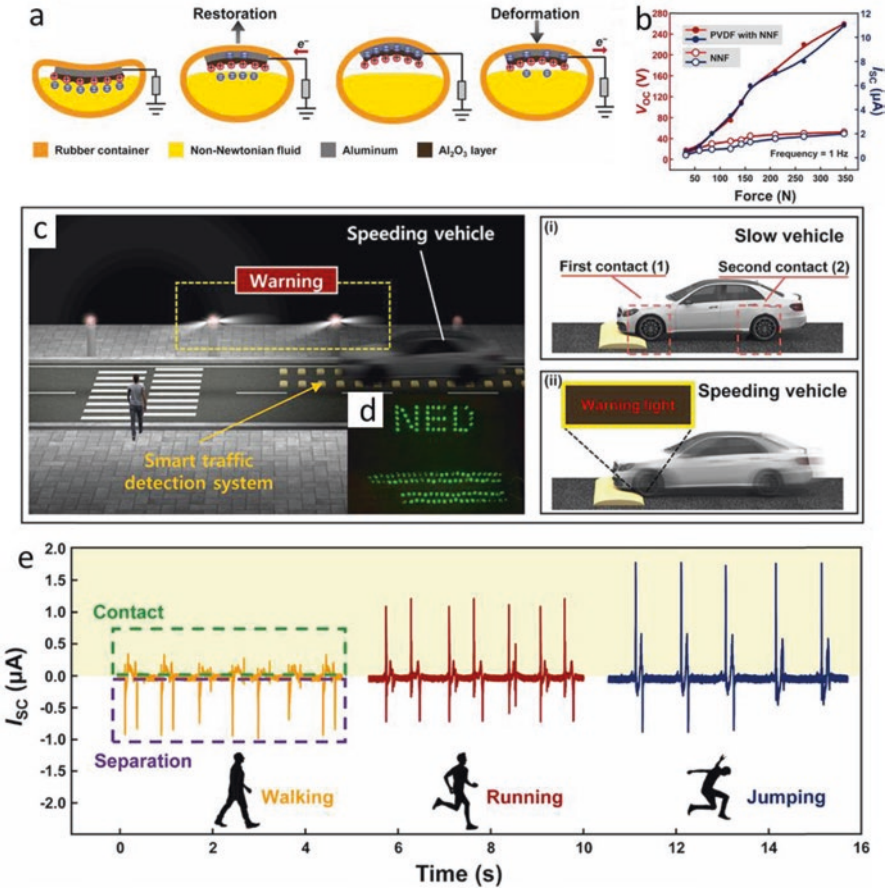


**Fig. 4.8** (**a**) Working mechanism of the proposed NNFT. (**b**) Electrical output generated from the NNFT-P with the various applied forces. (**c**) The schematic illustration of the proposed NSTDS and its working mechanism. (**d**) Photograph of the simultaneously turning 126 LEDs on using the electricity generated from the NNFT-P. (**e**) The electrical output according to walking, running, and jumping acquired from the NNFT-P [115]. Reprinted by permission from Elsevier

daily human movements such as finger sliding, touching, bending, hand shaking, knee bending, ankle bending, elbow bending, and hand tapping. These characteristics exhibit the potential of the STF-based TENG as a self-powered multi-functional device. Finally, STF-TENG can be used as an impact monitoring system connected to a smartphone that provided a warning upon receiving a strong pulse on the device.

Recently, Kim et al. [115] fabricated triboelectric nanogenerator (NNFT) using the non-Newtonian fluid (NNF) with shear thickening rheology. The prepared NNFT was operated in a single-electrode mode, consisting of cornstarch and

water-based suspension, aluminum electrode, and rubber container, respectively. The operating mechanism of the system is depicted in Fig. 4.8a. When the WAO-treated aluminum electrode is taken out from the STF for the rubber container restoration, the balanced state of the electrical equilibrium is disrupted due to the negative charge effect on the STF surface. For this reason, the electrons flow to the WAO-treated aluminum electrode from the ground to establish an electrical equilibrium between the $Al_2O_3$ layer and WAO-treated aluminum electrode. Upon completing the restoration, the electrical equilibrium is restored. By applying the external loading again, the negative charge effect appears on the WAO-treated aluminum electrode while the electrons are flowing from the WAO-treated aluminum electrode to the ground for retaining the electrical equilibrium. Consequently, the AC electricity is generated from the NNFT. The PVDF, which has a chemical formula of $(C_2H_2F_2)_n$, can enhance the triboelectricity due to the rich fluorine content in the PVDF. The NNFT-P with stronger friction point effect is obtained by mixing the STF with PVDF. Compared with the electrical output generated from the NNFT, the NNFT-P is enhanced by 5.41 times for the $V_{OC}$ while the increase is about 5.6 times for the $I_{SC}$ (Fig. 4.8b). Finally, a self-powered traffic detection system (NSTDS) based on NNFT-P is developed, which alerts the pedestrians to the danger (Fig. 4.8c-d). In addition, the developed NNFT-P can be employed as a sensor for motion detection such as walking, running, and jumping on the road (Fig. 4.8e).

Wang et al. [116] fabricated a textile-based TENG by including STF, graphene, and SSG with high performance fabrics. The TENG shows excellent energy-harvesting capabilities. The triboelectric properties of the TENG are investigated with an oscillator system. The effect of load amplitude and frequency on triboelectric performance is studied. As the force increases, the electrical signal increases (Fig. 4.9a). This is mainly due to the increased contact interface between the TENG and PMMA. Afterward, the corresponding voltage signals of TENG at different input frequencies are given in Fig. 4.9b, exhibiting a similar growing trend. This increase is caused by the reduction of separation time and the accumulation of more generated charges on the electrodes. The TENG shows a quite good electrical stability in one thousand loading and unloading excitation cycles (Fig. 4.9c). As a power unit, the TENG effectively provides a power for lightening up the LED array (Fig. 4.9d). It can also charge the commercial capacitors through rectifier circuits (Fig. 4.9e-f). The TENG shows enhanced protection properties under impact loadings. On the other side, the TENG can produce voltage signals due to the self-powered sensing effect (Fig. 4.9g). The negative peak voltage increases with the increase of descending height. In summary, the TENG not only shows a good impact resistance but also has a self-supplied power sensing performance at low-velocity impact conditions. In addition, the impact protection performance of the TENG under high-velocity impact is further studied. The toy in the pristine textile suit is completely penetrated, causing serious injuries. Instead, the bullet is effectively stopped by the TENG-based textile suit (Fig. 4.9h). This result proves that the ready

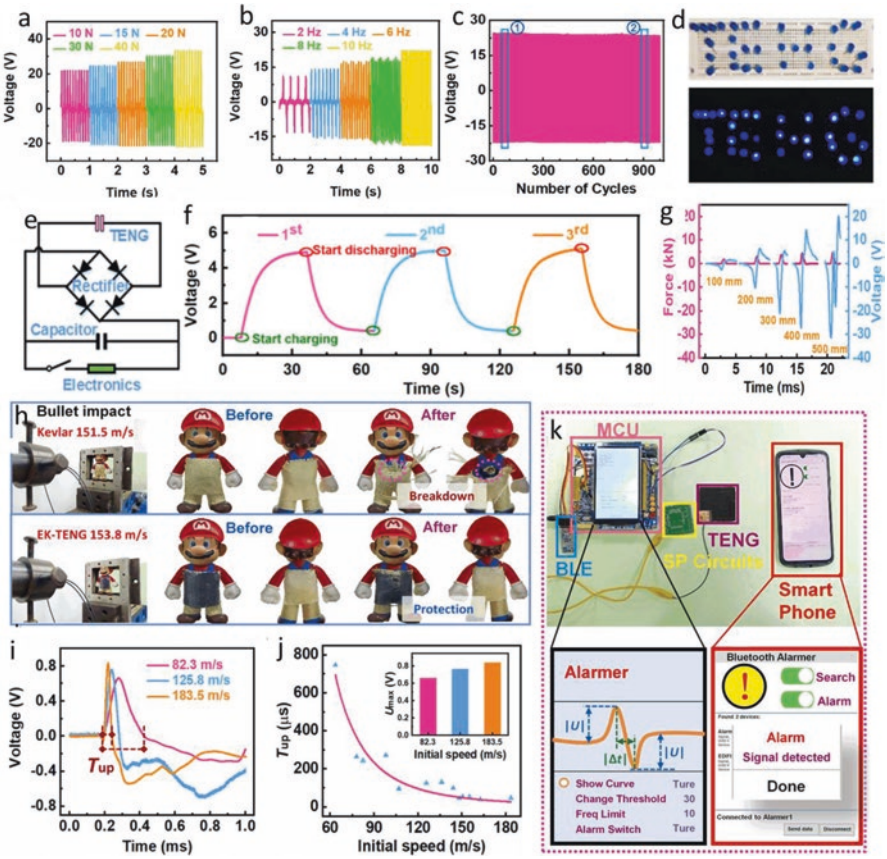


**Fig. 4.9** (**a**) Force-dependent output voltages at 10 Hz. (**b**) Frequency-dependent output voltages at 10 N. (**c**) Cycling stability of TENG at 10 MΩ. (**d**) TENG-harvested mechanical energy and lit up LEDs. (**e**) Rectifier circuit diagram for charging the capacitors. (**f**) The cycle charge-discharge curves of 0.47 μF capacitor by TENG at 40 N and 10 Hz. (**g**) The impact force and voltage vs. time with impactor dropping from 100 to 500 mm. (**h**) The scenario of safeguarding properties of TENG-based suit under high-speed shooting. (**i**) Voltage signals of TENG generated by the bullet impacts with 82.3, 125.8 and 183.5 m/s. (**j**) Impact velocity-dependent voltage positive peak duration time and maximum positive voltage. (**k**) The sensing system contained TENG-based Bluetooth and the interface of microcontroller and smartphone [116]. Reprinted by permission from Elsevier

TENG is able to prevent high-velocity impact damages. It is seen that the increase in the impact velocity leads to a rise in the peak voltage, while the duration of the positive voltage ($T_{up}$) also shows a significant reduction (Fig. 4.9j). The results indicate that the TENG has also good self-powered sensing capabilities under high-velocity impact. At the end, a TENG-based wireless passive sensor alarm system is developed, which is able to detect various kinds of impacting threats (Fig. 4.9k).

## 4.4 Conclusions

The unique mechanical properties of STFs provide important applications in a wide range of engineering and scientific fields. In this chapter, multi-function STF and multi-function system based on STF are discussed. According to the previous section, the STF can obtain the ability of multi-physical field coupling by changing the morphology, roughness, and surface characteristics of dispersed phase particles, or by adding additives. The force-thermal-coupled STF can change the shear thickening effect of STF by adjusting the temperature, which expands the application fields of STF. The color of the force-optical-coupled STF reflects the magnitude of the applied load, and the ability to change color under different conditions provides a wide range of potential applications for the STF in multi-functional soft armor defense materials. Moreover, STF with force-electric coupling characteristics shows high potential in the field of wearable protective devices.

Due to the special characteristics of STF, it can be used in different multi-functional devices. The STF-based electrolyte significantly improves the impact resistance and electrochemical stability of lithium batteries and supercapacitors, confirming its applicability to protect lithium ion batteries and supercapacitors from severe shocks. Nowadays, flexible sensors based on STF have been used in human motion detection and impact monitoring. Due to the high sensitivity, advanced impact resistance, and good flexibility, it is an important candidate for developing the next generation of sensors with protective properties. TENG is considered to be a promising energy conversion device because of its simplicity, lightweight, and low cost. The introduction of STF into TENG equipment enhances the structural durability and impact resistance of TENG equipment. Hence, smart STF fabrication with unique rheological and multi-field coupling properties, or design of multi-functional systems based on STF, proposes a broad application prospect in different engineering and scientific fields.

## References

1. W.H. Boersma, J. Laven, H.N. Stein, Shear thickening (dilatancy) in concentrated dispersions. AICHE J. **36**, 321–332 (1990)
2. Y.S. Lee, N.J. Wagner, Rheological properties and small-angle neutron scattering of a shear thickening, nanoparticle dispersion at high shear rates. Ind. Eng. Chem. Res. **45**, 7015–7024 (2006)
3. N.J. Wagner, J.F. Brady, Shear thickening in colloidal dispersions. Phys. Today **62**, 27–32 (2009)
4. Y.S. Lee, N.J. Wagner, Dynamic properties of shear thickening colloidal suspensions. Rheol. Acta **42**, 199–208 (2003)
5. R. Hoffman, Discontinuous and dilatant viscosity behavior in concentrated suspensions. II. Theory and experimental tests. J. Colloid Interface Sci. **46**, 491–506 (1974)

6. H.M. Laun, R. Bung, S. Hess, W. Loose, O. Hess, K. Hahn, et al., Rheological and small-angle neutron-scattering investigation of shear-induced particle structures of concentrated polymer dispersions submitted to plane Poiseuille and Couette flow. J. Rheol. **36**, 743–787 (1992)
7. J.W. Bender, N.J. Wagner, Optical measurement of the contributions of colloidal forces to the rheology of concentrated suspensions. J. Colloid Interface Sci. **172**, 171–184 (1995)
8. J. Bender, N.J. Wagner, Reversible shear thickening in monodisperse and bidisperse colloidal dispersions. J. Rheol. **40**, 899–916 (1996)
9. T.N. Phung, J.F. Brady, G. Bossis, Stokesian dynamics simulation of Brownian suspensions. J. Fluid Mech. **313**, 181–207 (1996)
10. R. Farr, J.R. Melrose, R. Ball, Kinetic theory of jamming in hard-sphere startup flows. Phys. Rev. E **55**, 7203–7211 (1997)
11. N.Y. Lin, B.M. Guy, M. Hermes, C. Ness, J. Sun, W.C. Poon, et al., Hydrodynamic and contact contributions to continuous shear thickening in colloidal suspensions. Phys. Rev. Lett. **115**, 228304 (2015)
12. R.L. Hoffman, Explanations for the cause of shear thickening in concentrated colloidal suspensions. J. Rheol. **42**, 111–123 (1998)
13. E. Brown, H.M. Jaeger, The role of dilation and confining stresses in shear thickening of dense suspensions. J. Rheol. **56**, 875–923 (2012)
14. D.P. Kalman, R.L. Merrill, N.J. Wagner, E.D. Wetzel, Effect of particle hardness on the penetration behavior of fabrics intercalated with dry particles and concentrated particle-fluid suspensions. ACS Appl Mater Inter **1**(11), 2602–2612 (2009)
15. A. Laha, A. Majumdar, Shear thickening fluids using silica-halloysite nanotubes to improve the impact resistance of p-aramid fabrics. Appl. Clay Sci. **132**, 468–474 (2016)
16. S. Gürgen, M.C. Kuşhan, The stab resistance of fabrics impregnated with shear thickening fluids including various particle size of additives. Compos Part A-Appl S **94**, 50–60 (2017)
17. S. Gürgen, M.C. Kuşhan, The ballistic performance of aramid based fabrics impregnated with multi-phase shear thickening fluids. Polym. Test. **64**, 296–306 (2017)
18. S.S. Cao, Q. Chen, Y.P. Wang, S.H. Xuan, W.Q. Jiang, X.L. Gong, High strain-rate dynamic mechanical properties of Kevlar fabrics impregnated with shear thickening fluid. Compos Part A-Appl S **100**, 161–169 (2017)
19. S.S. Cao, H.M. Pang, C.Y. Zhao, S.H. Xuan, X.L. Gong, The CNT/PSt-EA/Kevlar composite with excellent ballistic performance. Compos Part B-Eng **180**, 107793 (2020)
20. J.S. Zhang, Y. Wang, J.Y. Zhou, C.Y. Zhao, Y.X. Wu, S. Liu, et al., Intralayer interfacial sliding effect on the anti-impact performance of STF/Kevlar composite fabric. Compos Part A-Appl S **145**, 106401 (2021)
21. Q. Wang, R. Sun, M. Yao, M. Chen, Y. Feng, The influence of temperature on inter-yarns fictional properties of shear thickening fluids treated Kevlar fabrics. Composer Part A Appl S **116**, 46–53 (2019)
22. M.R. Sheikhi, S. Gürgen, Anti-impact design of multi-layer composites enhanced by shear thickening fluid. Compos. Struct. **279**, 114797 (2022)
23. S. Gürgen, F.A. Fernandes, R.J. Sousa, M.C. Kushan, Development of eco-friendly shock absorbing cork composites enhanced by a non-Newtonian fluid. Appl. Compos. Mater. **28**(1), 165–179 (2021)
24. Z.H. Tan, W.H. Li, W. Huang, The effect of graphene on the yarn pull-out force and ballistic performance of Kevlar fabrics impregnated with shear thickening fluids. Smart Mater. Struct. **27**(7), 075048 (2018)
25. M. Lin, C. Lou, J. Lin, T. Lin, J. Lin, Mechanical property evaluations of flexible laminated composites reinforced by high-performance Kevlar filaments: Tensile strength, peel load, and static puncture resistance. Compos Part B-Eng **166**, 139–147 (2019)
26. C. Fischer, S. Braun, P. Bourban, V. Michaud, C. Plummer, J.E. Månson, Dynamic properties of sandwich structures with integrated shear-thickening fluids. Smart Mater. Struct. **15**, 1467 (2006)

27. X. Zhang, W. Li, X. Gong, The rheology of shear thickening fluid (STF) and the dynamic performance of an STF-filled damper. Smart Mater. Struct. **17**, 035027 (2008)
28. S. Gürgen, M.A. Sofuoglu, Smart polymer integrated cork composites for enhanced vibration damping properties. Compos. Struct. **258**, 113200 (2021)
29. S. Gürgen, M.A. Sofuoglu, Vibration attenuation of sandwich structures filled with shear thickening fluids. Compos Part B-Eng **186**, 107831 (2020)
30. S. Liu, X.W. Fan, F. Yuan, M. Sang, J.Y. Zhou, J.S. Zhang, et al., Enabling thermally enhanced vibration attenuation via biomimetic Zr-fumarate MOF-based shear thickening fluid. Compos Part B-Eng **239**, 109964 (2022)
31. F. Pinto, M. Meo, Design and manufacturing of a novel shear thickening fluid composite (STFC) with enhanced out-of-plane properties and damage suppression. Appl Compos Mater **24**, 643–660 (2017)
32. A. Haris, B. Goh, T. Tay, H. Lee, A. Rammohan, V. Tan, On the effectiveness of incorporating shear thickening fluid with fumed silica particles in hip protectors. Smart Mater. Struct. **27**, 015021 (2017)
33. C.P. Hsu, J. Mandal, S.N. Ramakrishna, N.D. Spencer, L. Isa, Exploring the roles of roughness, friction and adhesion in discontinuous shear thickening by means of thermo-responsive particles. Nat. Commun. **12**(1), 1477 (2021)
34. Y.X. Wu, W.H. Wang, J.S. Zhang, M. Sang, Y.Q. Xu, J.Y. Zhou, et al., Liquid or solid? A biologically inspired concentrated suspension for protective coating. Chem. Eng. J. **428**, 131793 (2022)
35. M. Liu, W.Q. Jiang, S. Wang, S.H. Xuan, L.F. Bai, M. Sang, et al., Shear thickening fluid with tunable structural colors. Smart Mater. Struct. **27**, 095012 (2018)
36. J.B. Qin, B.R. Guo, L. Zhang, T.W. Wang, G.C. Zhang, X.T. Shi, Soft armor materials constructed with Kevlar fabric and a novel shear thickening fluid. Compos Part B-Eng **183**, 107686 (2020)
37. K.L. White, H. Yao, X. Zhang, H.J. Sue, Rheology of electrostatically tethered nanoplatelets and multi-walled carbon nanotubes in epoxy. Polymer **84**, 223–233 (2016)
38. R.B. Ladani, S.Y. Wu, A.J. Kinloch, K. Ghorbani, J. Zhang, A.P. Mouritz, et al., Multifunctional properties of epoxy nanocomposites reinforced by aligned nanoscale carbon. Mater Design **94**, 554–564 (2016)
39. X. Sha, K. Yu, H. Cao, K. Qian, Shear thickening behavior of nanoparticle suspensions with carbon nanofillers. J. Nanopart. Res. **15**(7), 1–11 (2013)
40. S. Gürgen, M.C. Kushan, W.H. Li, The effect of carbide particle additives on rheology of shear thickening fluids. Korea-Aust Rheol J **28**(2), 121–128 (2016)
41. B. Seifried, F. Temelli, Viscosity and rheological behavior of carbon dioxide-expanded fish oil fatty acid ethyl esters: Measurement using a rotational viscometer and modeling. J. Supercrit. Fluids **95**, 519–524 (2014)
42. J.S. Zhang, Y. Wang, H.X. Deng, J.Y. Zhou, S. Liu, J.P. Wu, et al., A high anti-impact STF/Ecoflex composite structure with a sensing capacity for wearable design. Compos Part B-Eng **233**, 109656 (2022)
43. S. Wang, S. Liu, J.Y. Zhou, F.X. Li, J. Li, X.F. Cao, et al., Advanced triboelectric nanogenerator with multi-mode energy harvesting and anti-impact properties for smart glove and wearable e-textile. Nano Energy **78**, 105291 (2020)
44. H.A. Barnes, Shear-thickening (dilatancy) in suspensions of nonaggregating solid particles dispersed in newtonian liquids. J. Rheol. **33**(2), 329–366 (1989)
45. H.G. Yang, C.Z. Li, H.C. Gu, T.N. Fang, Rheological behavior of titanium dioxide suspensions. J Colloid Interface Sci **236**(1), 96–103 (2001)
46. B.J. Maranzano, N.J. Wagner, The effects of particle-size on reversible shear thickening of concentrated colloidal dispersions. J. Chem. Phys. **114**(23), 10514–10527 (2001)
47. S.S. Zhang, Y.J. Zhang, H.W. Wang, Effect of particle size distributions on the rheology of Sn/ag/cu lead-free solder pastes. Mater Design **31**(1), 594–598 (2010)

48. R.G. Egres, F. Nettesheim, J. Wagnern, Rheo-SANS investigation of acicular-precipitated calcium carbon-ate colloidal suspensions through the shear thickening transition. J. Rheol. **50**(5), 685–709 (2006)
49. S. Majumdar, R. Krishnaswamy, A.K. Sood, Discontinuous shear thickening in confined dilute carbon nanotube suspensions. Proc. Natl. Acad. Sci. U. S. A. **108**(22), 8996–9001 (2011)
50. L.M. Zhang, T. Ma, J.L. Yang, Y. Huang, Rheological behavior of alumina suspensions. J. Inorg. Mater. **19**(5), 1145–1150 (2004)
51. M. Liu, Q. Chen, S. Wang, L.F. Bai, M. Sang, W.Q. Jiang, et al., PVP immobilized $SiO_2$ nanospheres for high-performance shear thickening fluid. J. Nanopart. Res. **19**, 234 (2017)
52. M. Liu, W.Q. Jiang, Q. Chen, S. Wang, Y. Mao, X.L. Gong, et al., A facile one-step method to synthesize $SiO_2$@polydopamine core-shell nanospheres for shear thickening fluid. RSC Adv. **6**, 29279–29287 (2016)
53. W.Q. Jiang, F. Ye, Q.Y. He, X.L. Gong, J.B. Feng, L. Lu, et al., Study of the particles' structure dependent rheological behavior for polymer nanospheres based shear-thickening fluid. J Colloid Interface Sci **413**, 8–16 (2014)
54. W.Q. Jiang, Y.Q. Sun, Y.L. Xu, C. Peng, X.L. Gong, Z. Zhang, Shear-thickening behavior of polymethyl-methacrylate particles suspensions in glycerine-water mixtures. Rheol. Acta **49**(11–12), 1157–1163 (2010)
55. Y. Otsubo, M. Fujiwara, M. Kouno, K. Edamura, Shear-thickening flow of suspensions of carbon nano-fibers in aqueous PVA solutions. Rheol. Acta **46**(7), 905–912 (2007)
56. H.L. Yang, J.M. Ruan, J.P. Zou, Q.M. Wu, Z.C. Zhou, Y.Y. Xie, Non-linear viscoelastic rheological properties of PCC/PEG suspensions. Chin. J. Chem. Phys. **22**(1), 46–50 (2009)
57. L. Albiston, K.R. Franklin, E. Lee, J. Smeulders, Rheology and microstructure of aqueous layered double hydroxide dispersions. J. Mater. Chem. **6**(5), 871–877 (1996)
58. S. Gürgen, W. Li, M.C. Kuşhan, The rheology of shear thickening fluids with various ceramic particle additives. Mater Design **104**, 312–319 (2016)
59. Y.L. Xu, X.L. Gong, C. Peng, Y.Q. Sun, W.Q. Jiang, Z. Zhang, Shear thickening fluids based on additives with different concentrations and molecular chain lengths. Chin. J. Chem. Phys. **23**, 342–346 (2010)
60. M. Kamibayashi, H. Ogura, Y. Otsubo, Shear-thickening flow of nanoparticle suspensions flocculated by polymer bridging. J. Colloid Interface Sci. **321**, 294–301 (2008)
61. G.V. Franks, Z.W. Zhou, N.J. Duin, D.V. Boger, Effect of interparticle forces on shear thickening of oxide suspensions. J. Rheol. **44**, 759–779 (2000)
62. F. Ye, W. Zhu, W.Q. Jiang, Z.Y. Wang, Q. Chen, X.L. Gong, et al., Influence of surfactants on shear-thickening behavior in concentrated polymer dispersions. J. Nanopart. Res. **15**, 2122 (2013)
63. X.Q. Liu, R.Y. Bao, X.J. Wu, W. Yang, B.H. Xie, M.B. Yang, Temperature induced gelation transition of a fumed silica/PEG shear thickening fluid. RSC Adv. **5**, 18367–18374 (2015)
64. J. Warren, S. Offenberger, H. Toghiani, C.U. Pittman, T.E. Lacy, S. Kundu, Effect of temperature on the shear-thickening behavior of fumed silica suspensions. ACS Appl. Mater. Interfaces **7**, 18650–18661 (2015)
65. T. Tian, G. Peng, W. Li, J. Ding, M. Nakano, Experimental and modelling study of the effect of temperature on shear thickening fluids. Korea-Aust Rheol J **27**, 17–24 (2015)
66. D. Rivero, L.M. Gouveia, A.J. Müller, A.E. Sáez, Shear-thickening behavior of high molecular weight poly(ethylene oxide) solutions. Rheol. Acta **51**, 13–20 (2012)
67. E. Yablonovitch, Inhibited spontaneous emission in solid state physics and electronics. Phys. Rev. Lett. **58**, 2059 (1987)
68. A. Blanco, E. Chomski, S. Grabtchak, M. Ibisate, S. John, S.W. Leonard, et al., Large-scale synthesis of a silicon photonic crystal with a complete three-dimensional bandgap near 1.5 micrometres. Nature **405**, 437–440 (2000)
69. M. Honda, T. Seki, Y. Takeoka, Dual tuning of the photonic band-gap structure in soft photonic crystals. Adv. Mater. **21**, 1801–1804 (2009)

70. A.C. Arsenault, D.P. Puzzo, I. Manners, G.A. Ozin, Photonic-crystal full-colour displays. Nat Photon **1**, 468–472 (2007)
71. W. Stöber, A. Fink, E. Bohn, Controlled growth of monodisperse silica spheres in the micron size range. J. Colloid Interface Sci. **26**, 62–69 (1968)
72. A.N. Golikand, E. Lohrasbi, M.G. Maragheh, M. Asgari, Carbon nano-tube supported Pt-pd as methanol-resistant oxygen reduction electrocatalyts for enhancing catalytic activity in DMFCs. J. Appl. Electrochem. **39**, 2421–2431 (2009)
73. M. Paradise, T. Goswami, Carbon nanotubes - production and industrial applications. Mater Design **28**, 1477–1489 (2007)
74. E. Svasand, K.D. Kristiansen, O.G. Martinsen, G. Helgesen, S. Grimnes, A.T. Skjeltorp, Behavior of carbon cone particle dispersions in electric and magnetic fields. Colloid Surf A **339**, 211–216 (2009)
75. O.S. Young, O.M. Kyung, K.T. Jin, Characterization and electrorheological response of silica/titania-coated MWNTs synthesized by sol-gel process. Colloid Surf A **436**, 354–362 (2013)
76. T. Makowski, M. Grala, W. Fortuniak, D. Kowalczyk, S. Brzezinski, Electrical properties of hydrophobic polyester and woven fabrics with conducting 3D network of multiwall carbon nanotubes. Mater Design **90**, 1026–1033 (2016)
77. A. Farjoud, E.A. Bagherpour, Electromagnet design for magneto-rheological devices. J Intel Mat Syst Str **27**(1), 51–70 (2016)
78. Y. Wang, S.H. Xuan, B. Dong, F. Xu, X.L. Gong, Stimuli dependent impedance of conductive magnetorheological elastomers. Smart Mater. Struct. **25**(2), 025003 (2016)
79. W. Xiaojie, F. Gordaninejad, M. Calgar, L. Yanming, J. Sutrisno, A. Fuchs, Sensing behavior of magnetorheological elastomers. J. Mech. Des. **131**(9), 091004 (2009)
80. M. Liu, S.S. Zhang, S. Liu, S.S. Cao, S. Wang, L.F. Bai, et al., CNT/STF/Kevlar-based wearable electronic textile with excellent anti-impact and sensing performance. Compos Part A-Appl S **126**, 105612 (2019)
81. M.A. Hannan, M.M. Hoque, A. Hussain, Y. Yusof, P.J. Ker, State-of-the-art and energy management system of lithium-ion batteries in electric vehicle applications: Issues and recommendations. IEEE Access **6**, 19362–19378 (2018)
82. L.G. Lu, X.B. Han, J.Q. Li, J.F. Hua, M.G. Ouyang, A review on the key issues for lithium-ion battery management in electric vehicles. J. Power Sources **226**, 272–288 (2013)
83. M.A. Hannan, M.S.H. Lipu, A. Hussain, A. Mohamed, A review of lithium-ion battery state of charge estimation and management system in electric vehicle applications: challenges and recommendations. Renew. Sust. Energ. Rev. **78**, 834–854 (2017)
84. G. Li, Z. Chen, J. Lu, Lithium-sulfur batteries for commercial applications. Chem **4**, 3–7 (2018)
85. Y. Wu, L. Yang, X. Tian, Y. Li, T. Zuo, Temporal and spatial analysis for end-of-life power batteries from electric vehicles in China. Resour. Conserv. Recycl. **155**, 104651 (2020)
86. M. Zarei, Portable biosensing devices for point-of-care diagnostics: Recent developments and applications. TrAC-Trends Anal Chem. **91**, 26–41 (2017)
87. A. Masias, J. Marcicki, W.A. Paxton, Opportunities and challenges of lithium ion batteries in automotive applications. ACS Energy Lett **6**(2), 621–630 (2021)
88. J. Benajes, A. García, J. Monsalve-Serrano, S. Martínez-Boggio, Emissions reduction from passenger cars with RCCI plug-in hybrid electric vehicle technology. Appl. Therm. Eng. **164**, 114430 (2020)
89. X. Duan, G. Naterer, Heat transfer in phase change materials for thermal management of electric vehicle battery modules. Int J Heat Mass Transf - Theory Appl **53**, 5176–5182 (2010)
90. R. Kizilel, A. Lateef, R. Sabbah, M. Farid, J. Selman, S. Al-Hallaj, Passive control of temperature excursion and uniformity in high-energy Li-ion battery packs at high current and ambient temperature. J. Power Sources **183**, 370–375 (2008)
91. R. Kizilel, R. Sabbah, J.R. Selman, S. Al-Hallaj, An alternative cooling system to enhance the safety of Li-ion battery packs. J. Power Sources **194**, 1105–1112 (2009)

92. J. Ding, T.F. Tian, Q. Meng, Z.P. Guo, W.H. Li, P. Zhang, et al., Smart multifunctional fluids for lithium ion batteries: Enhanced rate performance and intrinsic mechanical protection. Sci. Rep. **3**, 2485 (2013)
93. K.W. Liu, C.F. Cheng, L.Y. Zhou, F. Zou, W.F. Liang, M.Y. Wang, et al., A shear thickening fluid based impact resistant electrolyte for safe Li-ion batteries. J. Power Sources **423**, 297–304 (2019)
94. Y.X. Wu, S. Wang, M. Sang, Q. Shu, J.S. Zhang, S.H. Xuan, et al., A safeguarding and high temperature tolerant organogel electrolyte for flexible solid-state supercapacitors. J. Power Sources **505**, 0083 (2021)
95. Y. Wang, L. Wang, T. Yang, X. Li, X. Zang, M. Zhu, et al., Wearable and highly sensitive graphene strain sensors for human motion monitoring. Adv. Funct. Mater. **24**, 4666–4670 (2014)
96. Y. Yang, X. Yang, Y. Tan, Q. Yuan, Recent progress in flexible and wearable bio-electronics based on nanomaterials. Nano Res. **10**, 1560–1583 (2017)
97. X. Wang, Z. Liu, T. Zhang, Flexible sensing electronics for wearable/attachable health monitoring. Small **13**, 1602790 (2017)
98. H. Wang, H. Zhou, A. Gestos, J. Fang, H. Niu, J. Ding, et al., Robust, electro-conductive, self-healing superamphiphobic fabric prepared by one-step vapour-phase polymerisation of poly (3, 4-ethylenedioxythiophene) in the presence of fluorinated decyl polyhedral oligomeric silsesquioxane and fluorinated alkyl silane. Soft Matt **9**(1), 277–282 (2013)
99. D. Du, P. Li, J. Ouyang, Graphene coated nonwoven fabrics as wearable sensors. J Mater Chem C **4**(15), 3224–3230 (2016)
100. T.Q. Trung, N.E. Lee, Flexible and stretchable physical sensor integrated platforms for wearable human-activity monitoring and personal healthcare. Adv. Mater. **28**(22), 4338–4372 (2016)
101. R.E. Fernandez, Y. Umasankar, P. Manickam, J.C. Nickel, L.R. Iwasaki, B.K. Kawamoto, et al., Disposable aptamer-sensor aided by magnetic nanoparticle enrichment for detection of salivary cortisol variations in obstructive sleep apnea patients. Sci. Rep. **7**(1), 17992 (2017)
102. J. Kuang, Z. Dai, L. Liu, Z. Yang, M. Jin, Z. Zhang, Synergistic effects from graphene and carbon nanotubes endow ordered hierarchical structure foams with a combination of compressibility, super-elasticity and stability and potential application as pressure sensors. Nanoscale **7**(20), 9252–9260 (2015)
103. D. Vilarinho, A. Theodosiou, C. Leitão, A.G. Leal-Junior, M. Domingues, et al., POFBG-embedded cork insole for plantar pressure monitoring. Sensors **17**(12), 2924 (2017)
104. J. Wu, J. Wang, Y. Ling, H. Xu, An advanced hybrid technique of dcs and jsrc for tele monitoring of multi-sensor gait pattern. Sensors **17**(12), 2764 (2017)
105. W. Liu, J. Chen, Z. Chen, K. Liu, G. Zhou, Y. Sun, et al., Stretchable lithium-ion batteries enabled by device-scaled wavy structure and elastic-sticky separator. Adv. Energy Mater. **7**(21), 1701076 (2017)
106. S. Wang, L. Lin, Z.L. Wang, Triboelectric nanogenerators as self-powered active sensors. Nano Energy **11**, 436–462 (2015)
107. W.G. Kim, D.W. Kim, I.W. Tcho, J.K. Kim, M.S. Kim, Y.K. Choi, Triboelectric nanogenerator: Structure, mechanism, and applications. ACS Nano **15**(1), 258–287 (2021)
108. D.W. Kim, S.W. Kim, U. Jeong, Lipids: Source of static electricity of regenerative natural substances and nondestructive energy harvesting. Adv. Mater. **30**(52), 1804948 (2018)
109. K. Parida, V. Kumar, W. Jiangxin, V. Bhavanasi, R. Bendi, P.S. Lee, Highly transparent, stretchable, and self-healing ionic-skin triboelectric nanogenerators for energy harvesting and touch applications. Adv. Mater. **29**(37), 1702181 (2017)
110. J.Y. Zhou, S. Wang, F. Yuan, J.S. Zhang, S. Liu, C.Y. Zhao, et al., Functional kevlar-based triboelectric nanogenerator with impact energy-harvesting property for power source and personal safeguard. ACS Appl Mater Inter **13**, 6575–6584 (2021)
111. Y.T. Jao, P.K. Yang, C.M. Chiu, Y.J. Lin, S.W. Chen, D. Choi, et al., A textile-based triboelectric nanogenerator with humidity-resistant output characteristic and its applications in self-powered healthcare sensors. Nano Energy **50**, 513–520 (2018)

112. S. Wang, L. Ding, Y. Wang, X.L. Gong, Multifunctional triboelectric nanogenerator towards impact energy harvesting and safeguards. Nano Energy **59**, 434–442 (2019)
113. S. Wang, F. Yuan, S. Liu, J.Y. Zhou, S.H. Xuan, Y. Wang, et al., A smart triboelectric nanogenerator with tunable rheological and electrical performance for self-powered multi-sensors. J. Mater. Chem. C **8**, 3715–3723 (2020)
114. S.Y. Yun, I.W. Tcho, W.G. Kim, D.W. Kim, J.H. Son, S.W. Lee, et al., Mechanically robust triboelectric nanogenerator with a shear thickening fluid for impact monitoring. J. Mater. Chem. A **10**, 10383–10390 (2022)
115. Y. Kim, J. Yun, D. Kim, Robust and flexible triboelectric nanogenerator using non-Newtonian fluid characteristics towards smart traffic and human-motion detecting system. Nano Energy **98**, 107246 (2022)
116. W.H. Wang, J.Y. Zhou, S. Wang, F. Yuan, S. Liu, J.S. Zhang, et al., Enhanced Kevlar-based triboelectric nanogenerator with anti-impact and sensing performance towards wireless alarm system. Nano Energy **91**, 106657 (2022)